



# Solid-state effects of monofluorophenyl substitution in dithiadiazolyl radicals: Impact on S...S and S...N interactions and their classification *via* Hirshfeld surfaces and fingerprint plots

Jacqueline M. Cole<sup>a,b,\*</sup>, Christine M. Aherne<sup>c</sup>, Paul G. Waddell<sup>a,b</sup>, Arthur J. Banister<sup>c</sup>, Andrei S. Batsanov<sup>c</sup>, Judith A.K. Howard<sup>c</sup>

<sup>a</sup> Cavendish Laboratory, University of Cambridge, J.J. Thomson Avenue, Cambridge CB3 0HE, UK

<sup>b</sup> Department of Chemistry, University of New Brunswick, P.O. Box 4400, Fredericton, NB, Canada E3B 5A3

<sup>c</sup> Department of Chemistry, University of Durham, South Road, Durham DH1 3LE, England, UK

## ARTICLE INFO

### Article history:

Received 26 April 2012

Accepted 19 July 2012

Available online 27 July 2012

### Keywords:

Supramolecular

Sulfur–nitrogen

Structure–property relationships

Crystallography

Hirshfeld surfaces

## ABSTRACT

*Ortho*- and *para*-fluorophenyl 1,2,3,5-dithiadiazolyl (DTDA) radicals were synthesised and structurally characterised in the solid-state. This enables the well-known molecular origins of the electrical conductivity properties in this series of molecules to be studied, specifically S...S conduction pathways.

This work includes the first report of monofluorophenyl DTDA crystal structures, filling an important gap in the literature to complement the many structural records of di-, tri-, tetra- and pentafluorophenyl DTDA analogues. This report also overturns previous thinking that monofluoro-substitution in these phenyl DTDA compounds does not influence the supramolecular chemistry; indeed, we demonstrate that singular fluorine is indeed structurally (and therefore property) directing as per their di-, tri-, tetra- and pentafluorinated relatives. In particular, the S...S and S...N interactions that control the electrical conductivity in DTDA are distinct in these mono-fluorophenyl DTDA.

Hirshfeld surfaces were employed to clarify the nature and extent of these interactions. Their ability to exploit the very sensitive features of surface topologies in order to identify S...S and S...N intermolecular interactions is important since these interactions are much more subtle than, say, classical hydrogen-bonding.

Furthermore, we demonstrate that Hirshfeld surfaces can classify the entire set of intermolecular interactions for a compound *via* a fingerprint plot. This affords the instant recognition of a given type of DTDA supramolecular network. In turn, barcodes can be generated from these fingerprint plots which quantify the percentage contribution of atom pairs that are involved in intermolecular interactions within DTDA. The predictive potential of such classification within the field of molecular design is shown *via* a comparison of our fingerprint plots with those of DTDA from previous studies.

© 2012 Elsevier Ltd. All rights reserved.

## 1. Introduction

Exciting prospects for sulfur–nitrogen chemistry have been demonstrated by the unusual superconducting properties of poly-sulfurnitride [1] and the potential of DTDA radicals (Fig. 1) as ‘organic metal’ materials for magnetism and conduction. This has led to a sustained interest in their solid-state structure–property relationships [2–9]. It has been suggested that these useful properties, in particular the electronic conduction properties, are linked to the intermolecular, non-bonded, S...S contacts within the structures of these compounds. A large number of these compounds form co-planar dimers within their structures and it is

thought that the contacts between these dimers may take the form of a 4-centre 2-electron interaction where an electron pair is delocalised across the four sulfur atoms [10]. Stacking of DTDA rings forming continuous S...S contact chains is thought to facilitate electronic conduction in these compounds [2].

Previous studies into halogen-substituted phenyl-DTDA compounds have addressed the effect of the substituents on the reduction of dithiadiazolylum cations to form the corresponding radical [11]. Associated structural studies have investigated the modes of association (MA) of the S<sub>2</sub>N<sub>2</sub>C rings which form dimers (Fig. 2) and the S...N close contact motifs (Fig. 3) in bi- and trifluorophenyl DTDA radicals (SN) [12–16]. Intermolecular interactions in the structures reported by these studies have been rationalised by considering non-spherical van der Waals radii [17] and electrostatic potential maps [12].

Despite these studies, no structural investigation has been reported for monofluorophenyl DTDA radicals; indeed, only two

\* Corresponding author at: Cavendish Laboratory, University of Cambridge, J.J. Thomson Avenue, Cambridge CB3 0HE, UK. Tel.: +44 1223 337470.

E-mail address: [jmc61@cam.ac.uk](mailto:jmc61@cam.ac.uk) (J.M. Cole).

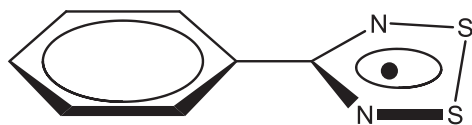


Fig. 1. Phenyl 1,2,3,5-dithiadiazolyl radical.

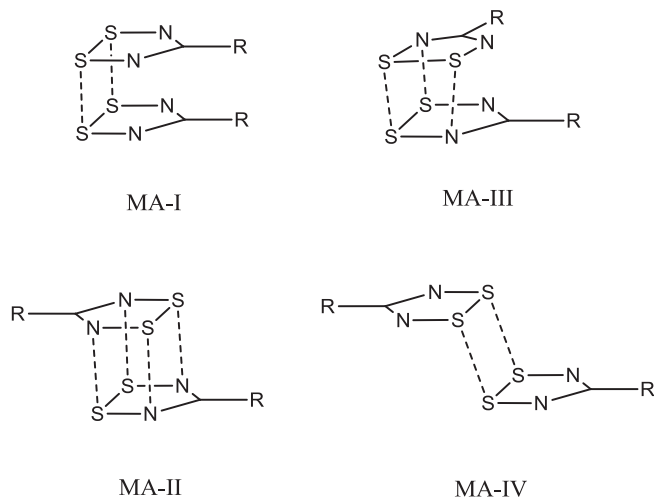


Fig. 2. Modes of association observed in DTDA radicals.

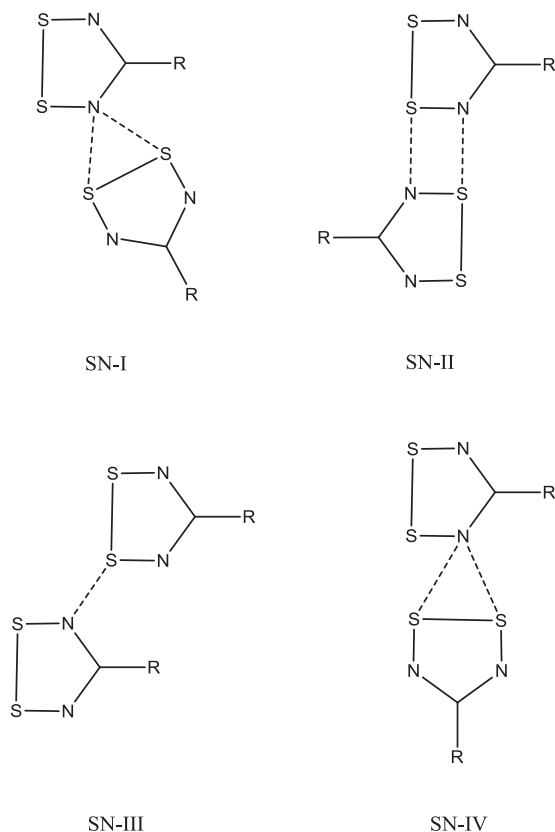


Fig. 3. S...N close contact motifs observed in DTDA radicals [11].

monohalogenated phenyl DTDA radicals (*para*-chloro- [18] and *para*-iodophenyl DTDA radicals [19]) have been structurally characterised and there is no such information for any *ortho*-monosubstituted derivative of the phenyl DTDA radical in the literature. Here we report the synthesis and X-ray structural characterisation

of *ortho*- and *para*-fluorophenyl-DTDA radicals and identify a new way to assess their intermolecular interactions by analysing Hirshfeld surfaces. Such an approach that has already proved most useful in identifying the intermolecular interactions in hydrogen-bonded structures [20–23]. Here, we extend this application to the identification of the more subtle types of intermolecular contacts that are observed in DTDA structures, with emphasis on non-bonded S...S contacts.

## 2. Experimental

### 2.1. Synthesis

Unless stated otherwise, all manipulations were performed in an inert atmosphere using standard Schlenk techniques. IR spectra were measured as Nujol mulls using a Perkin-Elmer 577 spectrophotometer. Microanalyses were carried out on a Carlo-Erba 1106 elemental analyser.

*para*-Fluorophenyl dithiadiazolyl radical ( $C_7H_4N_2FS_2$ , **1**) was synthesised via literature methods [24]. Single crystals suitable for X-ray crystallography were grown via sublimation of the product under vacuum at 373 K.

*ortho*-Fluorophenyl dithiadiazolyl radical ( $C_7H_4N_2FS_2$ , **2**): Lithium hexamethyldisilazane (1.39 g, 8 mmol) was dissolved in diethyl ether (40 mL) to which *ortho*-fluorobenzonitrile (0.90 g, 7.5 mmol) was added, producing a pale yellow solution. After stirring for 3 hours, sulfur dichloride (2.4 g, 23 mmol) was added to the now dark orange solution, affording a yellow solution, to which more solvent (25 mL) was added. The reaction was allowed to proceed overnight and then evaporated to dryness affording a yellow residue. The *ortho*-fluorophenyl dithiadiazolyl cation was removed from the residue via sulfur dioxide extraction leaving lithium chloride. The dark purple radical was then formed upon reduction by a Zn(Cu) redox couple (0.30 g, 4.61 mmol) in tetrahydrofuran. Single crystals suitable for X-ray crystallography were grown via sublimation of the product under vacuum at 373 K. *Elemental Anal.* (% calculated in brackets): C, 42.3 (42.2); H, 2.0 (2.0); N, 14.0 (14.1). IR:  $\nu_{max}$  1608m 1491w 1458s 1374s 1274w 1222w 1141m 1094m 1034w 908w 839w 804m 777s 763s 731m 652m 550m 511w.

### 2.2. X-ray crystallography

Crystal structure data for **1** and **2** (Tables 1 and 2) were collected at 150 K on a Rigaku AFC6S diffractometer equipped with

Table 1  
Experimental and refinement details for the X-ray structures of **1** and **2**.

	<b>1</b>	<b>2</b>
Fw	$C_7H_4FN_2S_2$	$C_7H_4FN_2S_2$
M	199.24	199.24
T (K)	150	150
Crystal system	monoclinic	monoclinic
Space group	$P2_1/n$	$P2_1/c$
a (Å)	5.7941(12)	13.327(6)
b (Å)	29.810(6)	18.183(6)
c (Å)	9.2007(18)	13.437(6)
$\alpha$ (°)	90	90
$\beta$ (°)	103.01(3)	107.37(3)
$\gamma$ (°)	90	90
U (Å <sup>3</sup> )	1548.4(5)	3108(2)
Z	8	16
$\mu$ (Mo K $\alpha$ ) (mm <sup>-1</sup> )	0.71073	0.71073
$D_{calc}$ (Mg m <sup>-3</sup> )	1.709	1.703
Total reflections	2022	5378
Independent reflections ( $R_{int}$ )	894 (0.079)	3578 (0.0631)
Final R, wR <sub>2</sub>	0.0484, 0.1255	0.0995, 0.3084
Largest difference: peak, hole (e Å <sup>-3</sup> )	0.384, -0.396	1.334, -0.879

**Table 2**  
Selected bond distances (Å) and angles (°) for **1** and **2**.

	Intramolecular S–S bond distances	Intramolecular S–N bond distances	Intradimer S...S contact distances	Interdimer S...S contact distances	Interplanar twist angle
<b>1</b>	S1–S2 2.093(3)	S1–N1 1.630(6)	S1...S3 3.055(3)	S1...S3 <sup>i</sup> 3.482(3)	<b>1</b> <sup>1</sup> 6.8(4)
	S3–S4 2.108(3)	S2–N2 1.628(6)	S2...S4 3.051(3)	S2...S4 <sup>i</sup> 3.354(3)	<b>1</b> <sup>2</sup> 6.3(5)
		S3–N3 1.638(6)			
		S4–N4 1.619(6)			
<b>2</b>	S1–S2 2.104(4)	S1–N1 1.628(9)	S1...S3 3.054(4)	S3...S6 3.403(3)	<b>2</b> <sup>1</sup> 11.8(4)
	S3–S4 2.100(4)	S2–N2 1.616(8)	S2...S4 3.078(4)	S4...S8 3.560(4)	<b>2</b> <sup>2</sup> 8.0(5)
	S5–S6 2.090(3)	S3–N3 1.632(8)	S5...S7 3.121(4)	S1...S6 <sup>ii</sup> 3.758(4)	<b>2</b> <sup>3</sup> 23.5(2)
	S7–S8 2.097(4)	S4–N4 1.638(9)	S6...S8 3.032(3)	S2...S8 <sup>ii</sup> 3.702(4)	<b>2</b> <sup>4</sup> 5.2(3)
		S5–N5 1.629(8)			
		S6–N6 1.613(7)			
		S7–N7 1.636(9)			
		S8–N8 1.616(9)			

(i)  $1/2 + x, 1/2 - y, 1/2 + z$ ; (ii)  $x, 1.5 - y, -0.5 + z$ .

a molybdenum X-ray source ( $\lambda_{\text{Mo K}\alpha} = 0.71073 \text{ \AA}$ ) and an Oxford Cryosystems Cryostream open-flow nitrogen cooling device.

The structures were solved by direct methods and refined by full-matrix least-squares methods on  $F^2$  values of all data. Refinements were performed using SHELXL [25]. Hydrogen atoms were positioned geometrically and refined as riding on their parent phenyl carbon atoms, with  $C-H = 0.950 \text{ \AA}$  and  $U_{\text{iso}}(H) = 1.2U_{\text{eq}}(C)$ . The structure of **2** shows substitutional disorder between opposing *ortho* F and H atoms and a high  $Z'$  value ( $Z' = 4$ ) results where two out of four of these molecules are disordered. There was no evidence for disorder in the other two asymmetric molecular units, nor was there any sign of twinning despite the fact that  $a \approx c$ , as can be a sign of twinning in a monoclinic crystal system. Its resulting  $R_1$  value is slightly high, as is a common observation in structures where  $Z' > 1$  [26]. Nonetheless, the model presents accurate bond geometry and meets all relevant checks for crystallographic integrity in Platon [27] such that we can be confident about its reliability.

### 2.3. Computational methods

Hirshfeld surfaces of the individual molecules of **1** and **2** have been calculated using CRYSTALEXPLORER 2.1 [28] in order to identify the important intermolecular interactions within the crystal structures [21,20,22]. Hirshfeld surfaces are representative of the electron distribution, calculated as the sum of the electron densities of isotropic atoms. Identification of close contacts is made possible via the normalised contact distance ( $d_{\text{norm}}$ ) relative to the distances from the surface to the nearest nucleus inside and outside the surface ( $d_i$  and  $d_e$  respectively) given by Eq. (1). These close intermolecular contacts *i.e.* those closer than van der Waals, are indicated by the corresponding red areas on the Hirshfeld surfaces of the molecules. In both **1** and **2**,  $Z' > 1$  and hence matching red spots are found on surfaces corresponding to different molecules.

$$d_{\text{norm}} = \frac{d_i - r_i^{\text{vdw}}}{r_i^{\text{vdw}}} + \frac{d_e - r_e^{\text{vdw}}}{r_e^{\text{vdw}}} \quad (1)$$

'Fingerprint' plots of each Hirshfeld surface were also derived from CRYSTALEXPLORER 2.1 by plotting  $d_i$  against  $d_e$ . Such figures allow one to classify a molecular set of intermolecular interactions according to a single topological characteristic. Breaking the surfaces down into percentage areas of the surface associated with specific interactions allows 'barcode' figures for each molecule to be produced, facilitating further this characterisation.

## 3. Results and discussion

### 3.1. Molecular and dimeric geometry

The crystallographic asymmetric unit (Fig. 4) of **1** comprises a dimer formed from two symmetry-independent molecules ( $Z' = 2$ ), that are related geometrically via a *cis*-cofacial arrangement (**MA-I**). The asymmetric unit of **2** (Fig. 5) comprises two dimers, denoted here by  $d^1$  and  $d^2$ ; all molecules therein are crystallographically independent ( $Z' = 4$ ). The dimer  $d^1$  lies perpendicular to (100) while  $d^2$  lies parallel to (100) and both exhibit the same **MA-I** mode of association. While  $d^2$  is ordered, the fluorine in  $d^1$  exhibits substitutional disorder in both molecules about the two possible *ortho*-positions in the phenyl ring. The fluorine atoms on each molecule that correspond to the dominant disordered component (70% for F1 and 85% for F3) lie on the same side of the dimer. For both **1** and **2**, the geometry of each crystallographically independent molecule is similar to those in previously reported fluoro-phenyl-substituted dithiadiazoyl (DTDA) compounds [12–16]. The two crystallographically independent molecules in **1** exhibit interplanar twist angles between the DTDA and phenyl rings of  $6.8(4)^\circ$  and  $6.3(5)^\circ$ . In **2**, the observed interplanar twist angles within each molecule of  $d^1$  are  $8.0(5)^\circ$  and  $11.8(4)^\circ$  while those observed in  $d^2$  are  $5.2(3)^\circ$  and  $23.5(2)^\circ$ . These geometries are also in line with previous findings.

The dimers observed in the structures of **1** and **2** are stabilised in the solid-state via intradimer S...S contacts (Table 2) and

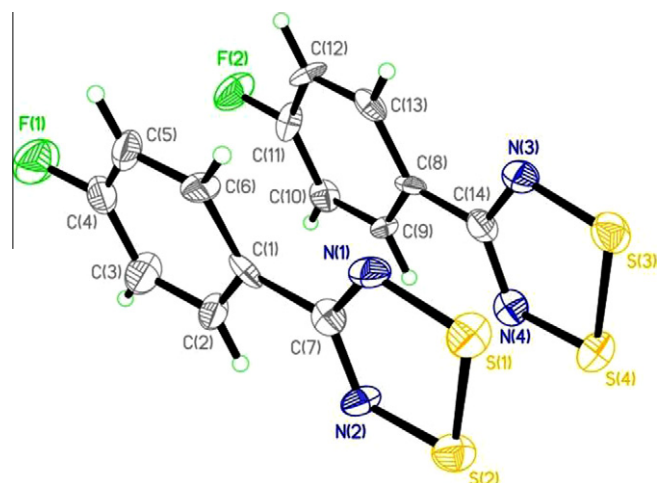


**Fig. 4.** Asymmetric unit of **1** with displacement ellipsoids drawn at the 50% probability level.

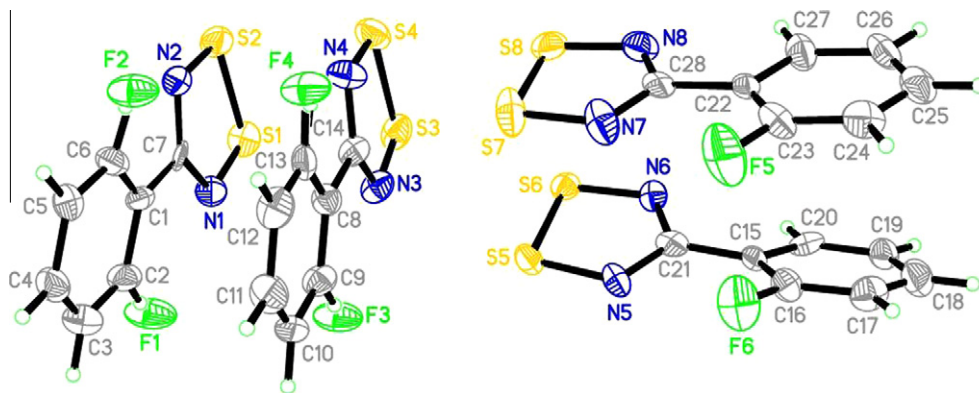


Fig. 5. Asymmetric unit of **2** with displacement ellipsoids drawn at the 50% probability level.

intradimer  $\pi\cdots\pi$  stacking interactions between the phenyl rings; in **1**, the centroid-centroid distance is 3.74(1) Å and in **2** the centroid-centroid distance is 3.64(1) Å for  $d^1$  and 3.79(1) Å for  $d^2$ . Close contacts between the C atoms of the radical ring (in **1**, C7...C14 3.281(9) Å; in **2**, C7...C14 3.31(1) Å and C21...C28 3.35(1) Å) are also apparent.

### 3.2. Crystal packing

Considering the interdimer S...S contacts in **1**, the dimeric units pack together forming chains in a 'herringbone' arrangement along [103] with the planes of the molecules lying parallel to (103) (Fig. 6). This differs from the very common pinwheel configuration seen in many of the fluorophenyl DTDA radicals [12,15] and the herringbone structure of 2,6-fluorophenyl DTDA where the dimers are arranged perpendicular to the direction of the motif [12]. These chains consist of linear [S...S...S] units that repeat in an alternating interdimer and intradimer fashion. The interdimer S...S distances lie at the shorter end of the range observed for similar 'in-plane' contacts in the bi- and trifluorophenyl analogues of these

compounds (3.361(3)–4.428(1) Å)<sup>12</sup>. The direction of the chains alternates along (010) forming staggered layers of molecules.

Continuous chains of alternating intra- and interdimer S...S contacts are also observed in the structure of **2**, though these form in a distinctly different way to those in **1**. The chains comprise alternate dimers lying perpendicular to each other, creating linear [S...S...S...S] units (Fig. 7). The chain then continues at right angles to this four-membered unit, much like the S...S contact chain observed in **1**, forming infinite chains of S...S contacts along [001]. These contacts are generally longer than those observed in **1** and hence there is less potential for electron hopping between dimers in **2**. Viewing the structure down [100], parallels can be drawn between **2** and the 'herringbone' chains observed in the structure of the monoclinic, dimeric polymorph of the 4-(2,6'-difluorophenyl)-DTDA radical [12]. The arrangement of  $d^2$  in **2** is similar to this dithiadiazolyl radical with the exception that the  $d^1$  dimer acts as a spacer oriented perpendicular to the  $d^2$  dimer lying parallel to (100). In this previously published structure, the S...N contact motif, identified as **SN-IV**, was attributed to close bifurcated S...N contacts. In this case, the same could be said of the structure of **2**

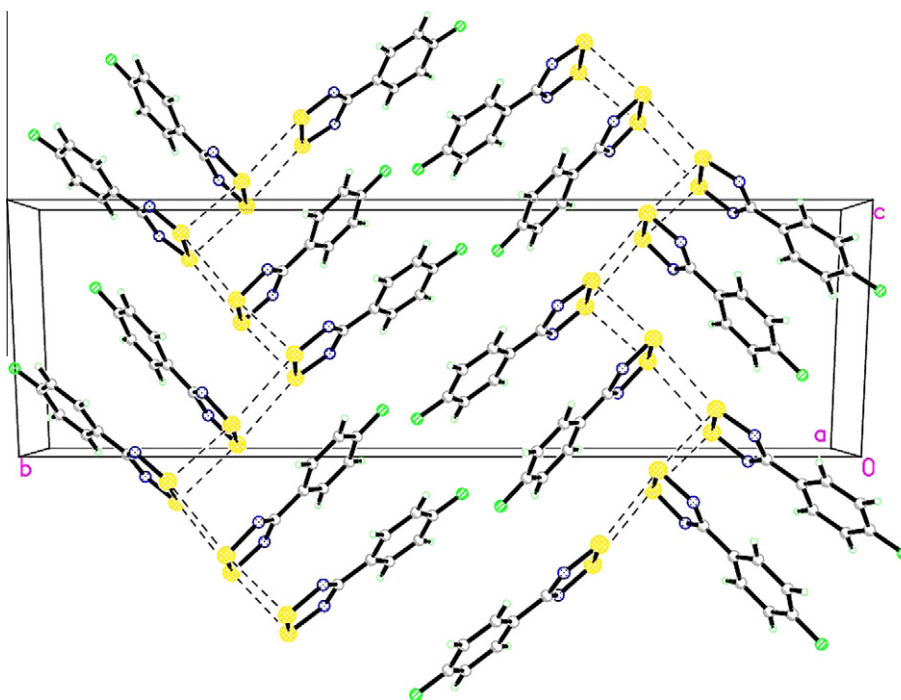


Fig. 6. Structure of **1** showing the chains formed via intermolecular S...S contacts (dashed lines) along [103].

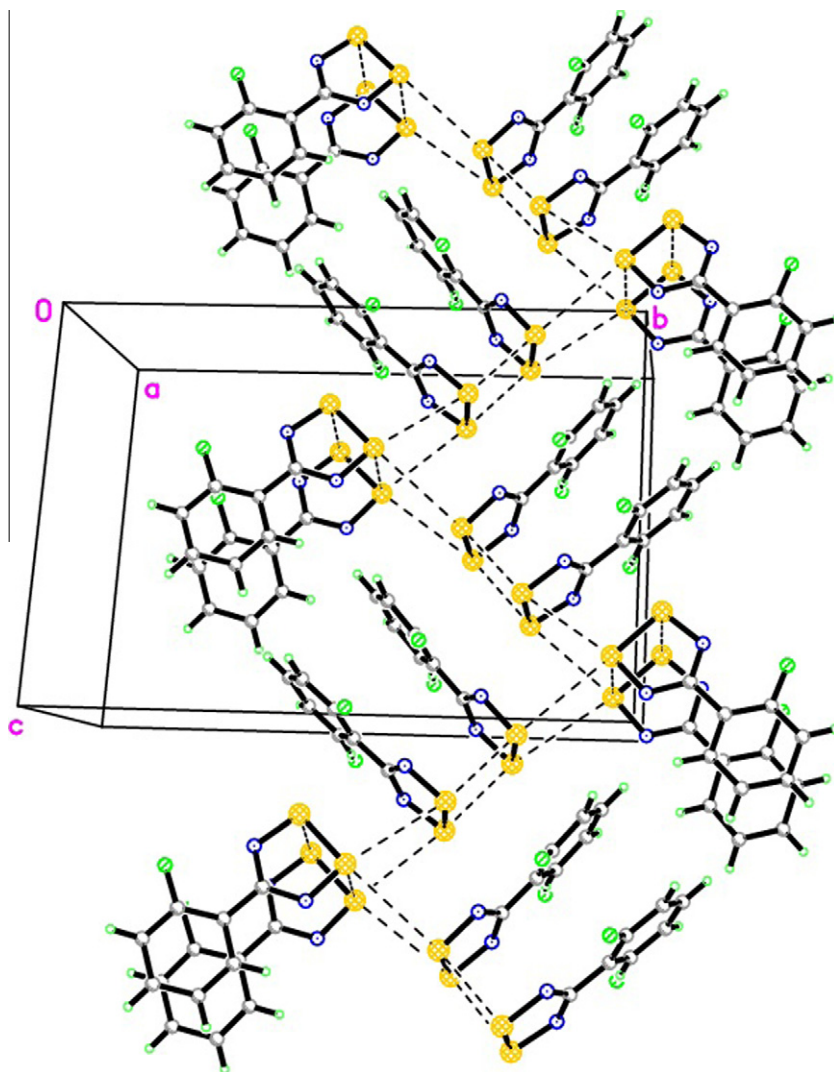


Fig. 7. Structure of 2 showing the chains formed via intermolecular S...S contacts (dashed lines) along [100].

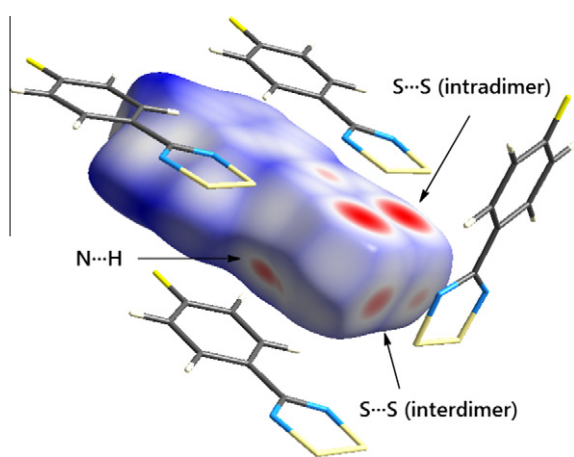


Fig. 8. Hirshfeld surface of molecule 1 of the structure of 1.

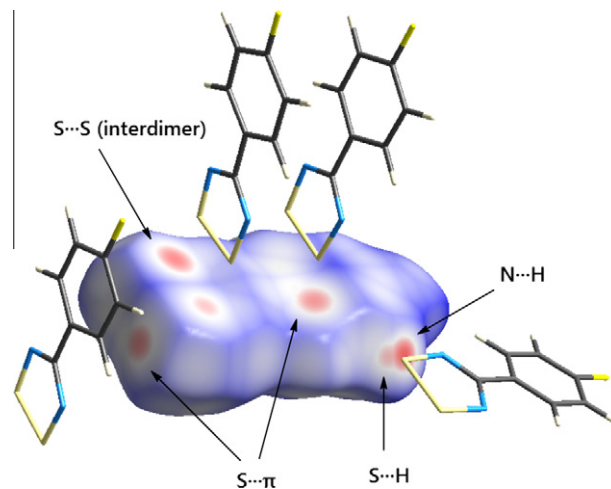


Fig. 9. Hirshfeld surfaces of molecule 2 of the structure of 1.

since the S...N distances (S5...N3 3.242(8) Å, S6...N3 3.395(8) Å, S7...N4 3.460(9) Å and S8...N4 3.56(1) Å) fulfil the criteria for close contacts given the sums of the van der Waals radii (3.20–3.63 Å) [12].

Examination of the Hirshfeld surfaces of the molecules in the structure of 1 (Figs. 8 and 9) demonstrates the significance of the S...S contacts both within and between dimers. This is despite

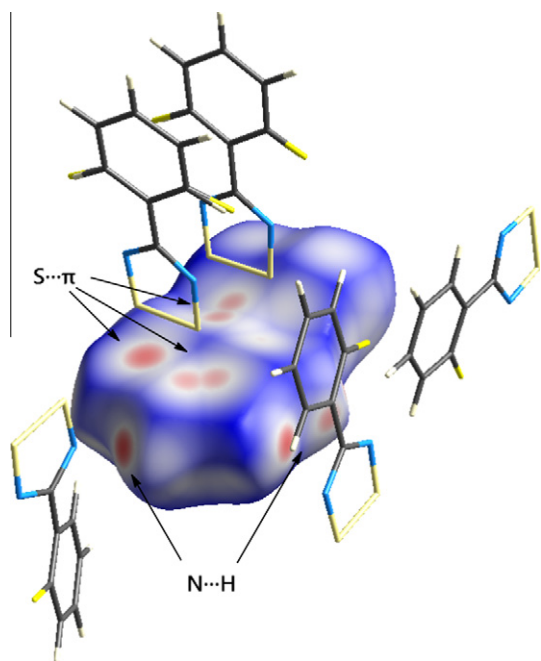


Fig. 10. Hirshfeld surfaces of molecule 1 of the structure of 2.

the methodology of Clarke et al. [12] through which  $S\cdots N$  contacts within the range of the sum of the van der Waals radii can be identified ( $S2\cdots N3$  3.481(7) Å,  $S2\cdots N1$  3.490(7) Å and  $S4\cdots N3$  3.469(7) Å) forming chains down [100] with a  $S\cdots N$  contact motif similar to **SN-III**. Yet, these interactions are not 'in-plane' owing to the staggered alignment of the chains of  $S\cdots S$  contacts.

Hirshfeld surfaces show that  $S\cdots N$  separations are not deemed to form close contacts. As such, the  $S\cdots S$  interactions dictate the crystal packing since they seem to form at the expense of  $S\cdots N$  contacts. A potential  $S\cdots\pi$  interaction is also highlighted by the Hirshfeld surfaces ( $S4\cdots C9$  3.302(6) Å, Fig. 9).

In **2**, analysis of the Hirshfeld surfaces (Figs. 10–13) indicates that the  $S\cdots S$  contacts are generally stronger than  $S\cdots N$  contacts and are likely to be more important in terms of the mode of association of the two dimers. What appear to be  $S\cdots N$  contacts are observed between two  $d^2$  dimers in a stacking arrangement ( $S6\cdots N6 = 3.501(7)$  Å), interacting via the **SN-II**  $S\cdots N$  contact motif.

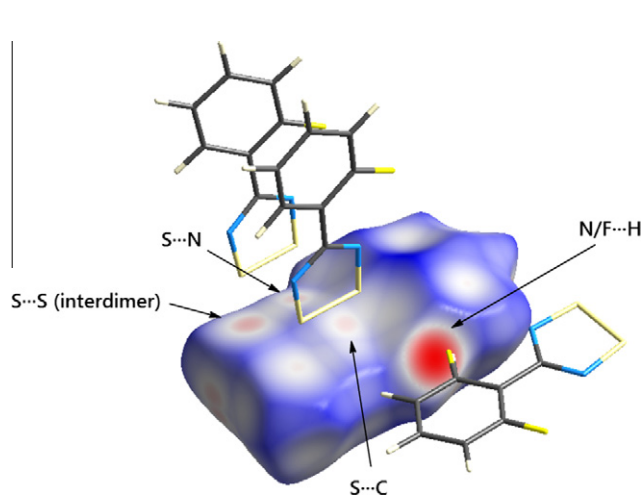


Fig. 11. Hirshfeld surfaces of molecule 2 of the structure of 2.  $N\cdots H$  and  $F\cdots H$  interactions (denoted by  $N/F\cdots H$ ) are difficult to delineate due to the manifest disorder.

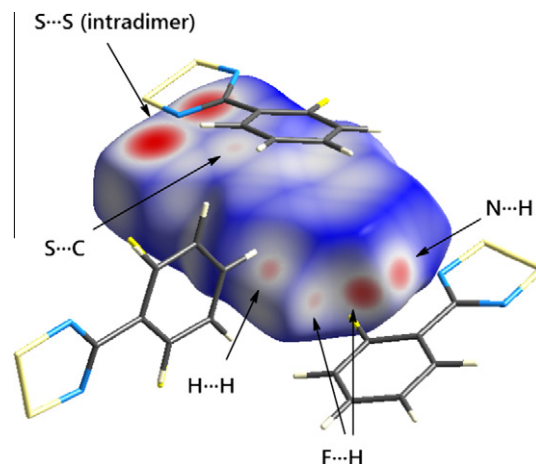


Fig. 12. Hirshfeld surfaces of molecule 3 of the structure of 2.

These interactions are not continuous in the manner of the stacking contacts in **1**, which form infinite stacks, but are finite connecting two of the planes parallel to (001). According to the Hirshfeld surfaces, there is little evidence for  $S\cdots N$  contacts since a red spot on the surface (indicative of a closer than van der Waals interaction) corresponding to this interaction is not observed. The close approach of these molecules for one half of the dimer appears to be due to  $S\cdots C$  close contacts ( $S6\cdots C21$  3.454(8) Å); the presence of these interactions over those of the more usual  $S\cdots N$  contacts in this family of compounds is most likely a consequence of steric effects rather than a more electrostatically favourable non-bonded interaction. In general, regarding Hirshfeld surfaces, it is clear that the intradimer contacts are much shorter than the interdimer contacts but the latter can be seen to be also significant, as evidenced by the corresponding red areas of the Hirshfeld surface. Though significant in a number of reported structures of bi- and tri-fluorophenyl radicals,  $S\cdots N$  contacts are not as prominent in the monofluorophenyl compounds. While it may be false to conclude that single F atoms produce little structure directing influence, as they play a role in many of the intermolecular interactions in the monofluorophenyl structures, it can be suggested that combinations of F atoms give rise specifically to structure-directing  $S\cdots N$  contacts whereas single F atoms do not.

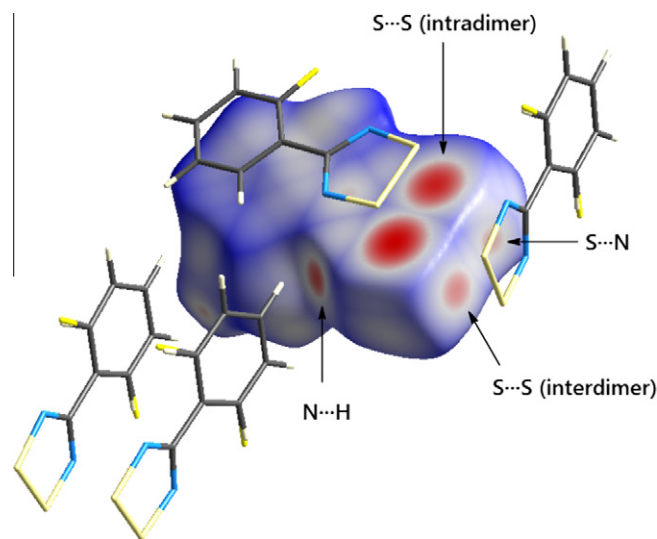
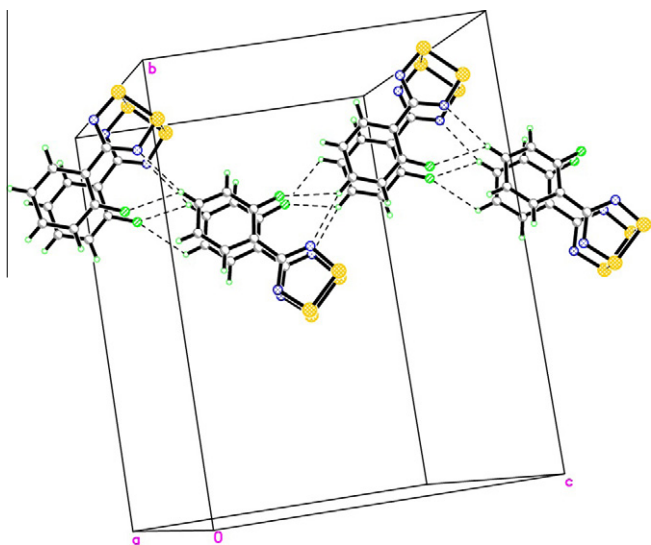


Fig. 13. Hirshfeld surfaces of molecule 4 of the structure of 2.



**Fig. 14.** Structure of **2** showing the chains formed *via* intermolecular F...H and N...H contacts (dashed lines) along [001].

H...F close contacts are observed in both structures in line with what was observed in other fluorophenyl DTDA's. In **1**, there are close contacts between *meta*-H and *para*-F atoms in opposing dimeric molecules which form about a crystallographic inversion centre (F1...H10 2.754(5) Å and F2...H3 2.793(4) Å). Since these interactions serve to link the chains of [S...S...S] units, it would

appear that the F atom presumably has a significant structure-directing influence. The chains of S...S contacts are similarly connected in the structure of **2**, in this case *via* bifurcated interactions between the *para*-H atoms and N and F atoms on adjacent, in-plane  $d^1$  dimers (N5...H18 = 2.614(7) Å and N7...H25 2.668(8) Å, F6...H18 2.669(6) Å and F5...H25 = 2.455(7) Å); these generate further chain motifs along [001] (Fig. 14). Similar interactions are a common feature of reported structures of this kind with *ortho*-fluorine atoms [12] and they are readily identified in this structure by analysis of the Hirshfeld surfaces (Fig. 12). An interaction between F5 and the *meta*-H of an adjacent radical (F5...H26 = 2.651(7) Å) is also apparent from the Hirshfeld surfaces. However, the distance between these atoms in analogous positions on the other radical comprising  $d^1$  is too long to be considered an interaction (F6...H19 = 3.169(6) Å), due to the greater interplanar twist angle observed for that radical. In turn, this twist angle can be attributed to repulsive H...H contacts between neighbouring  $d^1$  and  $d^2$  dimers. The H atoms appear to be brought into closer than the van der Waals range by a strong interaction between a N atom on  $d^1$  and a *para*-H on  $d^2$  (N6...H4 2.580(8) Å, Fig. 13).

Other potentially significant intermolecular interactions are also apparent in these structures. In **1**, close contacts occur as a result of the bifurcated interaction between a *meta*-H atom and S (S1...H10 3.002(2) Å) and N (N1...H10 2.646(7) Å) atoms, linking dimers along [010] (Fig. 9). Also present in the structure of **2** are a series of H...C and S...C contacts, the latter of which include some potential S... $\pi$  interactions (Fig. 10). Most interactions involving *ortho*-H and *ortho*-F atoms on  $d^1$  are not readily identifiable due to the occupational disorder, though the F2...H13 distance (2.38(4) Å) is the shortest F...H contact (Fig. 10).

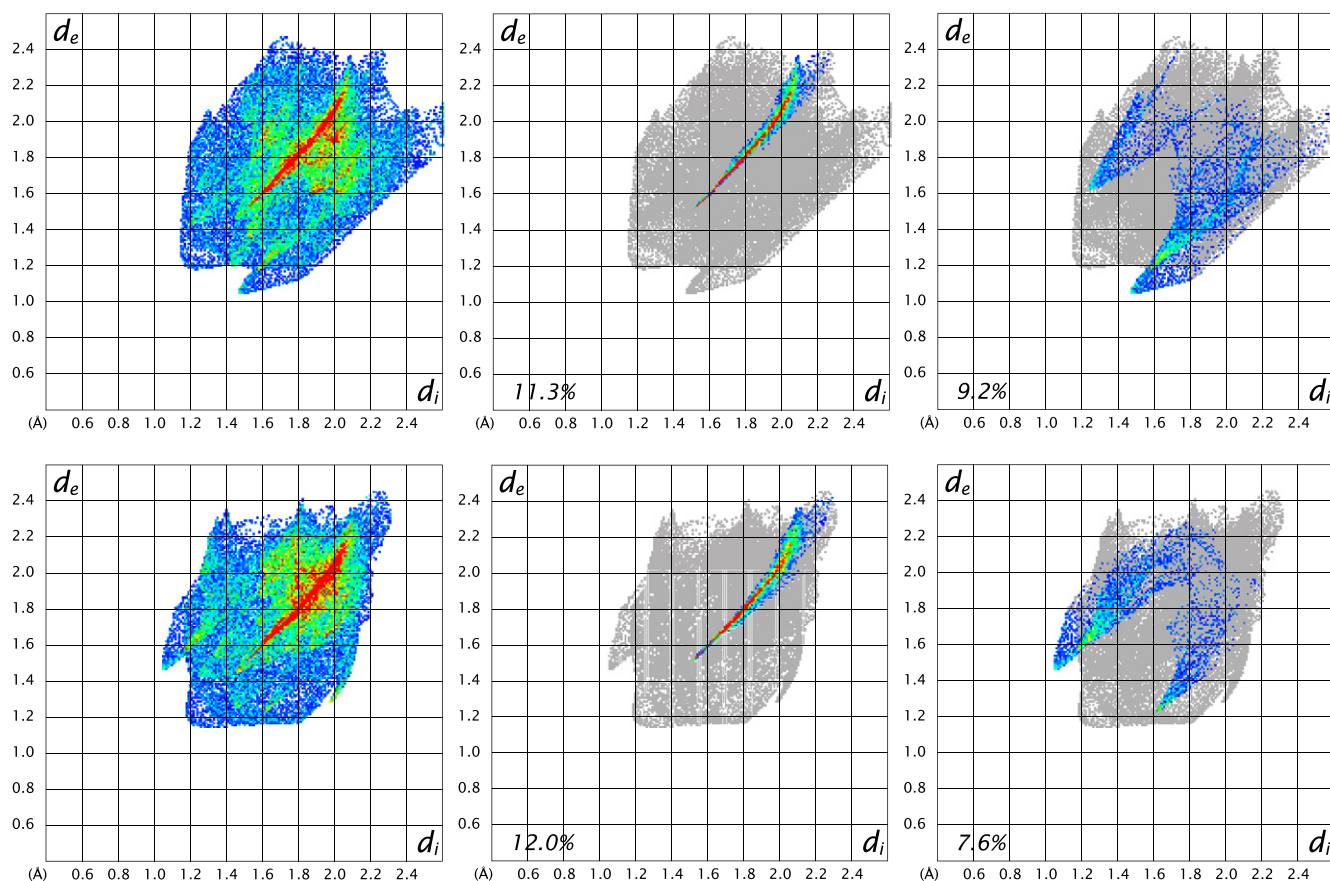


**Fig. 15.** Hirshfeld fingerprint plots for molecules **1** (top) and **2** (bottom) in **1** (showing all interactions (left), highlighting S...S interactions (middle) and highlighting N...H/H...N interactions (right)). Fingerprint plots for **2** are included in the supplementary material.

Comparing **1** with the two previously reported *para*-monohalogenated phenyl DTDA radicals, the chloro- and iodo-analogues of **1**, a comparison is best made between **1** and the chloro-analogue [18] since both exhibit the **MA-I** mode of association, whereas the iodo-analogue exhibits the **MA-II** mode of association [19]. However, the *para*-chlorophenyl DTDA radical does not form analogous S...S chain motifs to those observed in **1** in the solid-state. Close S...Cl contacts (S3...Cl2 3.385(5) Å and S4...Cl2 3.521(5) Å) are instead observed in the plane of the dimer containing the S atoms involved in the interaction.

Comparing the structure of **2** to that of the non-fluorinated phenyl DTDA radical [10,29], the impact of the *ortho*-fluorine substituent is clear. Both structures comprise four crystallographically independent molecules ( $Z = 4$ ) and hence two crystallographically independent dimers, which lie on different mean planes to each other. However, the discrete planes of molecules resulting from the formation of chains of S...S contacts in **2** are absent in the non-fluorinated form. It can be concluded that the aforementioned bifurcated interactions between the *para*-H atoms and N and F atoms along [001] (Fig. 14) exert their structure-directing influence by maintaining the discrete planes of molecules which assist in the formation of the S...S close contact motif.

### 3.3. Fingerprint plots

An overall summary of intermolecular contacts can be given by 2D fingerprint plots of the Hirshfeld surfaces produced by plotting  $d_i$  against  $d_e$  (e.g. Fig. 15) [20]. The most striking common characteristic of the fingerprint plots of **1** and **2** are the intense red streaks in the centre representing S...S contacts. Stubby 'wings' are visible in each fingerprint plot of **1** (Fig. 15) starting at  $d_e \approx 1.0$  and  $d_i \approx 1.5$  for molecule 1 where the N atom is participating and *vice versa* in molecule 2. These wings represent N...H interactions between the two molecules; similar peaks can be seen in the fingerprint plots for the molecules of **2** as well as those corresponding to F...H, C...H and S...H interactions.

Breaking down the Hirshfeld surface of **1** into percentage areas associated with a particular atom-type...atom-type interaction affords interaction 'barcodes' (Fig. 16). These barcodes reveal that S...S interactions account for *ca.* 12% of interactions for both molecules of **1** and 9–10% of molecules of **2** highlighting the longer interdimer S...S contacts observed in **2**. The importance of H...H interactions is readily identifiable here since they account for, respectively, 17.7% and 15.5% of the Hirshfeld surface for molecules 1 and 2 (which comprise  $d^1$ ). The larger percentage of S...H and S...C interactions in molecule 2 compared to molecule 1 reflect the end-on S... $\pi$  mode of association seen between two examples

of molecule 2. Very low percentages of N...N interactions are observed in both molecules in spite of the *cis*-cofacial arrangement of the molecules in the dimers. Though interestingly, despite there being no readily identifiable close S...N contacts, S...N interactions account for 6.7% and 12.4% of the Hirshfeld surface in molecule 1 and 2 respectively.

Fewer H...H interactions are apparent on the surfaces of molecules in **2** (Fig. 17) but the bifurcated N...H interactions in molecules 3 and 4 (which comprise  $d^2$ ) are evidenced by the increase in percentage of N...H interactions for these molecules relative to both **1** and **2**. Again, the relatively low percentage of S...N contacts is notable.

Generating analogous interaction 'barcodes' for the previously reported fluorophenyl DTDA structures (provided in the supplementary information) [12–16,29] allows a number of important observations to be made. Firstly, regarding S...N interactions, their Hirshfeld surface percentage contribution does not appear to follow any trend as far as the presence of structure-directing close contacts are concerned. For example, the mono-fluorinated compounds **1** and **2**, which exhibit no or few S...N close contacts contain similar percentages of S...N interactions to those bi- and tri-fluorinated compounds where these close contacts are observed.

Secondly, and more importantly as far as potential conducting properties are concerned, the Hirshfeld surface area percentages of S...S contacts observed in each molecule afford a direct indication of the mode of association and motif within the structure, as higher percentages can be associated with continuous S...S contact motifs. Those compounds which exhibit the 'pinwheel' motif as well as those exhibiting direct stacking of dimers with the **MA-I** mode of association [12–16,29], both of which result in infinite chains of S...S contacts, have much higher percentages of S...S contacts (*ca.* 9–15%) than those without these motifs or where other modes of association are observed (*ca.* 3–8%). These percentages could serve as a quantitative prediction of electrical conducting potential. The high percentage barcode values observed in **1** and **2** (*ca.* 9–12%) are therefore indicative of their S...S contact motifs; though the lower values observed in **2** compared to **1** may indicate a lower potential for conduction properties, most likely a result of its longer inter-dimer S...S contacts.

In terms of structural prediction, the use of electrostatic isopotentials, as per the methodology of Clarke et al. [12], has limited usefulness for predicting the structures of monofluorinated DTDA radicals, as evidenced by the structures of **1** and **2** reported herein. However, it remains valid in terms of predicting structural motifs in similar DTDA radicals. It also has the distinct advantage over Hirshfeld surfaces that it can predict structural motifs simply from a chemical sketch of the molecule. Indeed, Hirshfeld surfaces can

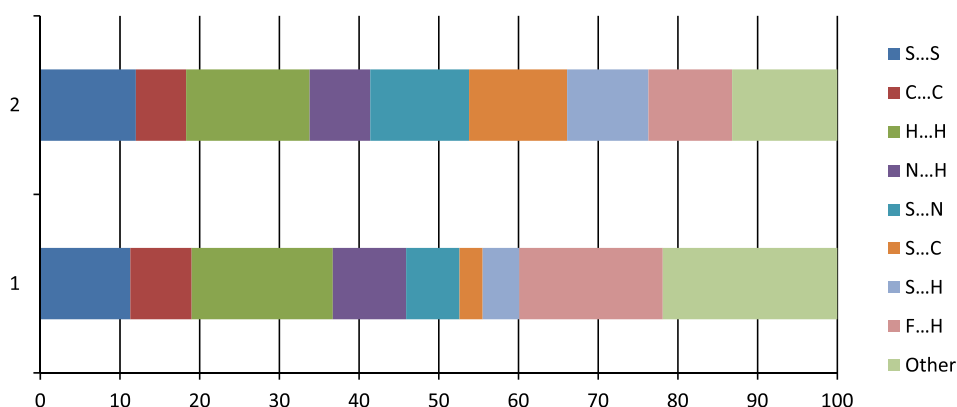
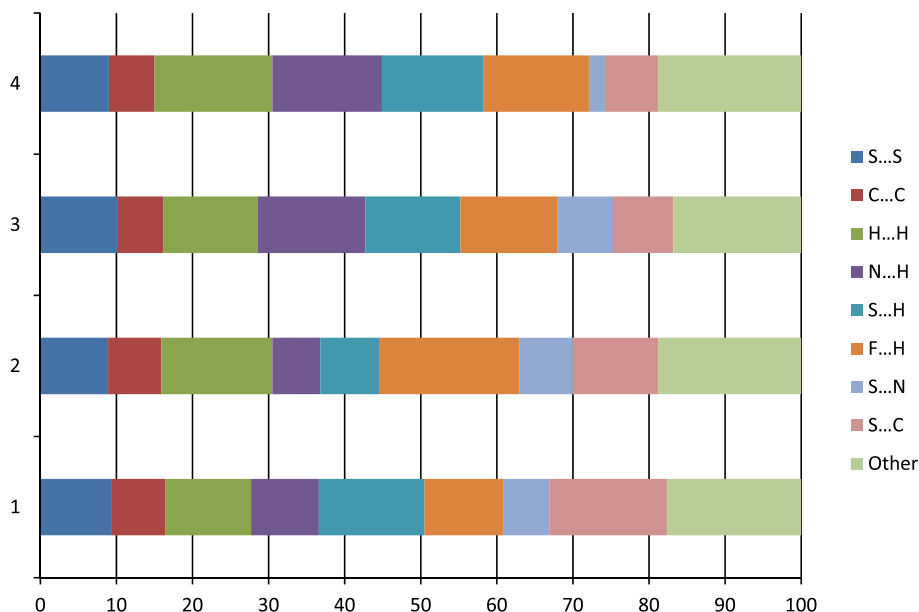


Fig. 16. Barcode chart showing the breakdown of the intermolecular interactions for the two independent molecules of **1**. Each atom-type/atom-type interaction given includes reciprocal contacts.



**Fig. 17.** Barcode chart showing the breakdown of the intermolecular interactions for the four independent molecules of **2**. Each atom-type/atom-type interaction given includes reciprocal contacts.

only be generated from *a priori* known crystal structures, where the structural motif is of course already known, so rendering its prediction moot. Instead, Hirshfeld surfaces act to rationalise rather than predict structural motifs, as demonstrated herein. Nevertheless, Hirshfeld surfaces represent a highly complementary predictive tool to this electrostatic isopotential approach in that they can predict *properties* of these structural motifs. It is in this sense that Hirshfeld surfaces demonstrate potential use in the design of new DTDA materials with tailor-made functional properties.

#### 4. Concluding remarks

Our analysis of two monofluorophenyl DTDA radicals refutes the previous assertion that one fluorine atom alone does not possess much structure-directing ability [12]. Indeed, the positioning of the *ortho*- or *para*-fluorine in **1** and **2** appears to dictate the appearance of structural motifs. Considering intermolecular contacts involving nitrogen atoms in DTDA radicals, however, it can be said that more than one fluorine is necessary to produce a large enough  $\delta^-$  charge on N to allow for strong N...X contacts, as the monofluorophenyl DTDA radicals do not exhibit as many close contacts involving N atoms compared to their bi- and trifluorophenyl counterparts.

We have also demonstrated that Hirshfeld surfaces are a very useful tool for visualising intermolecular interactions in these molecules where such contacts appear subtle and yet, they are easily identifiable by this method. Moreover, their relative strengths are easily gauged allowing for simple rationalisation of the most important, structure-directing interactions. Deriving fingerprint plots and barcode graphs from these surfaces can also help to evaluate the potential of these compounds as electrical conductors since they represent an ensemble classification of non-bonded contacts *via* the partitioning of Hirshfeld surface areas into intermolecular interaction percentage contributions; and higher Hirshfeld surface area percentages of S...S contacts are indicative of infinite S...S contact motifs.

Such classification affords the concept of performing systematic large-scale comparisons of non-bonded contacts in DTDA

materials. This leads to the prospect of employing smart material design strategies with this ‘training’ data, to predict DTDA materials that have designer S...S contacts, in order to realise their potential as electrical conductors.

#### Acknowledgements

J.M.C. thanks the Royal Society for a University Research Fellowship, the University of New Brunswick for the UNB Vice-Chancellor’s Research Chair and NSERC for the Discovery Grant 355708 (for P.G.W.).

#### Appendix A. Supplementary data

CCDC 878564 and CCDC 878565 contain the supplementary crystallographic data for **1** and **2**, respectively. These data can be obtained free of charge *via* <http://www.ccdc.cam.ac.uk/conts/retrieving.html>, or from the Cambridge Crystallographic Data Centre, 12 Union Road, Cambridge CB2 1EZ, UK; fax: (+44) 1223-336-033; or e-mail: [deposit@ccdc.cam.ac.uk](mailto:deposit@ccdc.cam.ac.uk). Supplementary data associated with this article can be found, in the online version, at <http://dx.doi.org/10.1016/j.poly.2012.07.066>.

#### References

- [1] C.-H. Hsu, M.M. Labes, *J. Chem. Phys.* 61 (1974) 4640.
- [2] J.M. Rawson, A.J. Banister, I. Lavender, *Adv. Heterocycl. Chem.* 62 (1995) 137.
- [3] A.W. Cordes, R.C. Haddon, R.T. Oakley, *Phosphorus Sulfur Silicon Relat. Elem.* 179 (2004) 673.
- [4] R.C. Haddon, *Nature* 256 (1975) 394.
- [5] L. Ducasse, *Chem. Phys. Lett.* 352 (2002) 454.
- [6] J.M. Rawson, A. Alberola, A. Whalley, *J. Mater. Chem.* 16 (2006) 2560.
- [7] D.A. Haynes, *CrystEngComm* 13 (2011) 4793.
- [8] J.M. Cole, C.M. Aherne, J.A.K. Howard, A.J. Banister, P.G. Waddell, *Acta Crystallogr., Sect. E Struct. Rep. Online* 67 (2011) o2514.
- [9] C.D. Martin, P.J. Ragogna, *Annu. Rep. Prog. Chem. Sect. A Inorg. Chem.* 107 (2011) 110.
- [10] A. Vegas, A. Pérez-Salazar, A.J. Banister, R.G. Hey, *Dalton Trans.* (1979) 1812.
- [11] C.M. Aherne, A.J. Banister, T.J. Hibbert, A.W. Luke, J.M. Rawson, *Polyhedron* 16 (1997) 4239.
- [12] C.S. Clarke, D.A. Haynes, J.N.B. Smith, A.S. Batsanov, J.A.K. Howard, S.I. Pascux, J.M. Rawson, *CrystEngComm* 12 (2010) 172.

- [13] A.J. Banister, A.S. Batsanov, O.G. Dawe, P.L. Herbertson, J.A.K. Howard, S. Lynn, I. May, J.N.B. Smith, J.M. Rawson, T.E. Rogers, B.K. Tanner, F. Palacio, Dalton Trans. (1997) 2539.
- [14] A.M.T. Bell, J.N.B. Smith, J.P. Attfield, J.M. Rawson, K. Shankland, W.I.F. David, New J. Chem. 23 (1999) 565.
- [15] L. Beer, A. Wallace Cordes, D.J.T. Myles, R.T. Oakley, N.J. Taylor, CrystEngComm 2 (2000) 109.
- [16] E.M. Fatila, M.C. Jennings, J. Goodreid, K.E. Preuss, Acta Crystallogr., Sect. C Cryst. Struct. Comm. 66 (2010) o260.
- [17] S.C. Nyburg, C.H. Faerman, Acta Crystallogr., Sect. B Struct. Sci. B41 (1985) 274.
- [18] R.T. Boeré, K.H. Moock, M. Parvez, Z. Anorg. Allg. Chem. 620 (1994) 1589.
- [19] N. Bricklebank, S. Hargreaves, S.E. Spey, Polyhedron 19 (2000) 1163.
- [20] M.A. Spackman, D. Jayatilaka, CrystEngComm 11 (2009) 19.
- [21] F.P.A. Fabbiani, L.T. Byrne, J.J. McKinnon, M.A. Spackman, CrystEngComm 9 (2007) 728.
- [22] H.F. Clausen, M.S. Chevallier, M.A. Spackman, B.B. Iversen, New J. Chem. 34 (2010) 193.
- [23] S.K. Seth, G.C. Maity, T. Kar, J. Mol. Struct. 1000 (2011) 120.
- [24] C.M. Aherne, A.J. Banister, I.B. Gorrell, M.I. Hansford, Z.V. Hauptman, A.W. Luke, J.M. Rawson, Dalton Trans. (1993) 967.
- [25] G.M. Sheldrick, Acta Crystallogr., Sect. A Found. Crystallogr. 64 (2008) 112.
- [26] D.J. Watkin, Crystallogr. Rev. 16 (2010) 197.
- [27] A.L. Spek, Acta Crystallogr., Sect. A Found. Crystallogr. A46 (1990) C34.
- [28] S.K. Wölf, D.J. Grimwood, J.J. McKinnon, D. Jayatilaka, M.A. Spackman, CRYSTALEXPLORER 2.1, University of Western Australia, Perth, Australia, 2007.
- [29] C. Allen, D.A. Haynes, C.M. Pask, J.M. Rawson, CrystEngComm 11 (2009) 2048.